5. SPECTROMETER PERFORMANCE

5.1 Systematic and Random Error Sources

The performance of a spectrometer is judged by the absolute accuracy of the measured attenuation and refractivity. A key question is how reliably can one deduce from recorded s_{11} data the parameters that enter into (17) to (21). Two different circumstances govern absorption and refraction detection:

Attenuation α relies on distortion-free, repeatable detection of resonance responses, which specify either Q values, **Q** and Q° (15), or a resonance strength S_R and an amplitude factor, g_x (16). Interfering fluctuations are limited, to first order, to the scan period of 2 s. Both parameter sets, derived with different NLS methods (see Table 3) yielded comparable results, although for the production runs the F3 scheme was used exclusively.

Refractivity N′ depends on the stability characteristics of the resonator center frequency f_x as a function of temperature drift and pressure loading over measurement periods lasting from minutes to hours. The ANA guarantees high frequency stability.

Precise temperature control and solid resonator construction are mandatory to ensure a drift-free and pressure insensitive value for f_x. Typically, the ANA-based detection scheme allowed about 100 Hz frequency resolution, which leads to taxing requirements for the mechanical integrity of the resonator structure. Most of the non-repeatable measurement errors originate from physical changes in the resonator structure during the progression of an experiment. For example, the length d_R has to remain stable to within ±0.33 nm (!) over the time period of a measurement sequence (1 to 5 hrs). During this period the temperature is fluctuating; in addition, the pressure is changing, which loads the structure, introduces temperature gradients, and bends the vacuum window. The latter might tune the resonator and affect the coupling, which changes Q_c or S_R.

Cell temperature T_c was monitored with ±1°C accuracy and ±0.001°C resolution. The measured coefficient of thermal tuning at 60 GHz was

$$(\delta f_x/f_x/\delta T = 0.68 \quad \text{ppm/°C}. \tag{24}$$

The positive sign follows from the coefficient of thermal expansion for the two brass mirrors (18 ppm/°C) plus steel micrometer (11.7 ppm/°C), which shortens d_R with temperature. This decrease is not fully overcome by expansion of the invar spacers (- 0.8 ppm/°C). Resonator structure and surrounding cell walls possess a large thermal time constant (≥ 15 min), which ensures thermal stability. The cell was kept at a constant temperature by a proportional controller using a precision platinum probe (circulator bath, assisted below 35°C by a cooled thermal exchanger). Ambient temperature fluctuated typically by ±3°C, which translated into a temperature stability for the cell of $\Delta T/\Delta t \approx \pm 0.01$°C/min ≈ ±0.1°C/day, thus causing some slow drift of f_x. According to (21) and (24), changes of a few millidegrees lead to noticeable (≥ 100 Hz) drifts. The correction term N_c of (22) is a measure of the drift between start and finish of a run.

Gas pressure P was measured by a differential capacitance manometer with 0.2 percent error, and its absolute calibration was periodically compared with a precision (±0.2 percent) quartz Bourdon-type manometer. The resonator structure is mechanically rugged and is not affected by pressure differentials; however, there is some compressibility in the micrometer thread and a small bending of the quartz window. Pressure stability of the resonator was tested at ten frequencies between 58 and 66 GHz by performing 12-step pressure scans, P = 0 to 110 kPa, introducing loss-free nitrogen. Systematic pressure-induced, erroneous attenuation readings were not observed within the limits, $\alpha \leq \pm 0.1$ dB/km. From refractivity results for dry air and the known constant r_G (3), the pressure loading influence upon f_x was estimated to be

$$(\delta f_x/f_x)/\delta P \approx -\, 6.5\times10^{-5} \quad \text{ppm/kPa}, \tag{25}$$

which translates for P = 0 to 101 kPa at 60 GHz into a change of - 490 Hz.

Mechanical tuning could be reproduced to within $\delta f_x \approx \pm 75$ kHz due to the resolution (δd_R) of the micrometer reading. When the resonator is mechanically tuned by changing d_R and then returned to its former position, the resonance parameters f_x, g_x, and S_R are not exactly replicated due to very small tilts in the mirror alignment. In addition, vibrations can affect the physical structure of the resonator, thus modulating the resonance response. In summary, foremost mechanical distortions of the resonator structure, related to temperature and pressure changes during a measurement period, lead to both systematic and random errors.

5.2 Signal Simulation

The spectrometer output s_{11} contains the reflected signal from the resonator and the noise spectra from both RF and LO sources. The two synthesized, identical generators of the ANA system have exceptionally clean spectra even after 5× (RF) and 14× (LO) multiplications. The complex reflection scattering coefficient, s_{11}, is determined by five parameters, a′, a″; f_x, **Q** and Q° (15) or a′, a″; f_x, g_x and S_R (16). These parameter sets were determined by NLS fits.

The residuals of a particular fit were examined for deterministic trends. In Figure 8, their real and imaginary parts from five-parameter fits to s_{11} parameters (scale ±0.001, in units of $|s_{11}| = 0$ to 1) are plotted over a frequency span $\Delta f = 5b_x$ for three cases:

(a) Simulation with pure white noise (pseudo-random, Gaussian distributed variations with a standard deviation, $\sigma_s = 0.0003$) added to a normalized (a′ = - 1, a″ = 0, S_R = 5 kHz, g_x = 20, f_x = 0) resonance. Note, how these residuals appear to be white noise

(b) Example at 58.1 GHz (α = 1.30 dB/km), which resembles case (a), and which can be interpreted to represent the amplitude/phase noise level of the ANA ($\sigma_s = 0.00028$)

c) Example at 61.8 GHz (α = 6.48 dB/km), which exhibits a distinct deterministic component yielding $\sigma_s = 0.00087$; here, a five-parameter fit of the detected, somewhat asymmetric s_{11} response is not sufficient to emulate the signal. Attenuation measurements were not affected by σ_s (≤ 0.001); asymmetry effects seem to cancel (difference in equation 20).

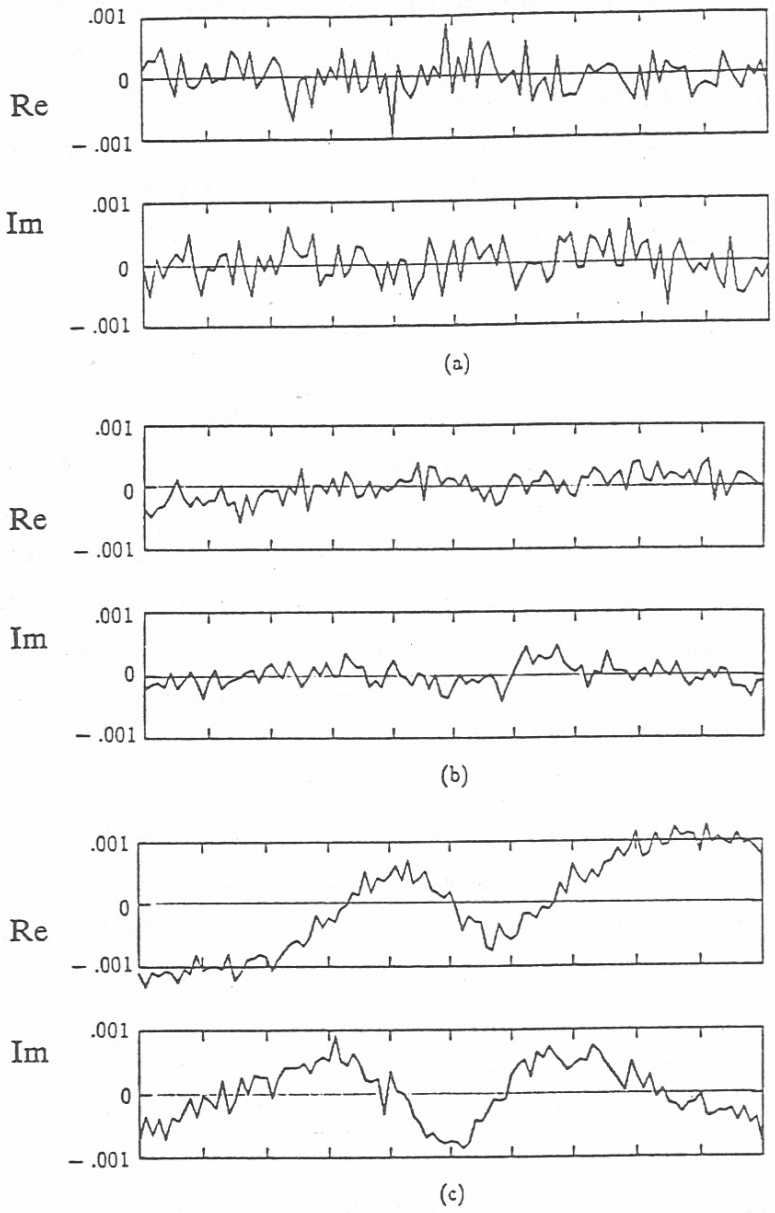

Figure 8. Three examples of real and imaginary parts of the point-by-point (101pts) residuals $\delta s_{11}(\Delta f)$:
(a) Simulated s_{11}, assuming random fluctuations
(b) Experimental s_{11} (58.1 GHz, 12.1 kPa air, 30°C), good response symmetry around f_x
(c) Experimental s_{11} (61.8 GHz, 47.2 kPa air, 30°C), poor response symmetry around f_x
(b,c are F2-fits).

5.3 Measurement Procedure

Up to this point, individual performances of various spectrometer elements have been evaluated. A typical measurement sequence for dry air measurements involves eight steps:

S1 - spectrometer cell is evacuated and thermally stable

S2 - resonator is mechanically tuned to an initial frequency f_0^i, value of q is determined from knowing d_R

S3 - coupling is tuned (l_c), multiple (up to 15×) consecutive (e.g., q = 71 to 85) resonances are excited

S4 - main program is started, ANA operating conditions (pts, avg) are selected, a data file name is created, the first center frequency is tuned in, and automatically (cursor is set to the peak: value under computer control) centered over the span $\Delta f = f_0 \pm 250$ kHz

S5 - resonance response is defeated by turning a motor-driven metal vane (rotary vacuum feedthrough) into the field region. ANA performs a "response" calibration for a short, which sets over the span Δf the signal level to $s_{11} = 1 + j0$. When the calibration is completed, the vane turns aside, and $s_{11}(\Delta f)$ data (51 pts, 128 avg) are recorded ten times to obtain a statistical average (see Table 6). The process is repeated for each f_0^i

S6 - air is introduced into the spectrometer cell, a piezo-activated valve opens and the gas pressure slowly rises until a computer-set pressure value P is reached

S7 - measurement sequence is completed after having stepped through fixed P values selected to increase from 0 to 101 kPa

S8 - cell is slowly evacuated by the operator, the resonator is mechanically retuned, and the next sequence is started.

5.4 Measurement Examples

The first example is for f = 55.7 GHz (q = 75) and T = 29.4°C. Ten s_{11} sets were individually fitted to (16) and statistically evaluated (F3). Table 7 exhibits the measurement protocol, of which one result is shown here in detail:

ANA Signal $a' = -0.999\,517(50)$ and $a'' = 0.000\,17(11)$.

Resonance Strength $S_R = 1.2667(52)$ kHz.

Center frequencies and amplitude factors

$P_0 = 0.0$ kPa	:	$f_0 = 55\,672\,046.18(39)$ kHz,	$g_0 = 83.91(06)$
P = 101.3 kPa	:	$f_x = 55\,657\,524.40(43)$,	$g_x = 106.75(16)$
$P_0 = 0.0$ kPa	:	$f_0 = 55\,672\,034.43(17)$,	$g_0 = 84.07(13)$.

Attenuation rates, computed with (20):

vacuum reference, $P_0^f - P_0^i$ (RE)	$\alpha_0 = 0.04(03)$,	
dry air	$\alpha_x = 5.27(05)$;	
MPM89 prediction	$\alpha_M = 5.41$ dB/km.	dB/km.

Refractivity, computed with (21):

total		N_x = 260.845(12),
resonator drift		N_c = 0.211(09);
MPM89 predictions	(nondispersive)	N_s = 259.965,
	(dispersive)	N' = 0.669 ppm.

Assuming $N_x' = N'$, yields with (23) r_x = 0.98050(6).

The measured refractivity factor r_x agrees with the accepted value, r_{Air} (3).

The second example is for f = 60.7 GHz (q = 82), T = 6.7°C:

ANA Signal a' = - 0.999 703(24) and a'' = - 0.00138(18).

Resonance Strength S_R = 6.6259(81) kHz.

Center frequencies and amplitude factors

P_0 = 0.0 kPa	:	f_0 = 60 685 426.881(84) kHz,	g_0 = 15.093(04),
P = 101.4 kPa	:	f_x = 60 668 016.5(11),	g_x = 28.608(18),
P_0 = 0.0 kPa	:	f_0 = 60 685 465.376(96),	g_0 = 15.079(03),

Attenuation rate, computed with (20):

vacuum reference (RE)	α_0 = - 0.02(01) = 0.00(03),
dry air	α_x = 16.31(03);
MPM89 prediction	α_M = 16.63 dB/km.

Refractivity, computed with (21):

total		N_x = 286.896(19),
resonator drift		N_C = - 0.634(02);
MPM89 predictions	(nondispersive)	N_s = 282.225,
	(dispersive)	N' = - 0.401 ppm.
Assuming $N_{f,x} = N_f$, yields with (23)		r_x = 1.0009(8).

The refraction factor r_x is about 2 percent larger than r_{Air}. Additional instrumental tuning was caused by the mechanical coupler to the tuning micrometer, which transmitted pressure bending of the vacuum chamber to the resonator structure. This problem was eventually corrected; however, the earlier refractivity results above 60 GHz proved unreliable (see Sect. 6.2).

When the refractive dispersion N' is known from model predictions (e.g., at $f_x \approx 60$ GHz: $N' \approx 0$), one obtains from (3),(23) a refractivity constant $R_s = 792.06 \cdot r_{Air}$ = 776.24 ppm·K/kPa for dry air. This constant provides a check on the correct measurement of the gas density ($\propto$ P/T). A few selected results (e.g., f_x = 60.0 GHz, P = 101 kPa) for the difference N_x - N'(MPM89) revealed a systematic trend Δ which is indicative of small, temperature-dependent errors in either the pressure or the temperature measurement:

T (°C)	R_s (ppm·K/kPa)	Δ (%)
6.7	780.0	0.55
29.7	776.3	0.00
52.4	772.6	-0.48.

Table 6

Example of Statistical Averaging at 62.5 GHz (51pts/128avg):

- Results (f_0, g_0, S_R, and a′,a″) of an F3-fit to (16)
- Correlation Coefficients $\rho_1(f_0 \rightarrow g_0)$, $\rho_2(f_0 \rightarrow S_R)$, and $\rho_3(g_0 \rightarrow S_R)$
- Standard Deviation of the Residuals, σ_s

	f_0 (Hz)	g_0	S_R (Hz)	a′	a″	σ_s		
62.5 GHz,	.0 torr,	29.8 C.						
	62500443913.	15.876	6579.8	-.999735	-.000429	.00059		
	178.	.029	29.3	.000116	.000060	.004	-.011	-.388
	62500444409.	15.874	6577.6	-.999724	-.000557	.00058		
	175.	.029	27.7	.000113	.000059	.004	-.010	-.388
	62500444662.	15.886	6589.4	-.999743	-.000703	.00063		
	191.	.032	30.4	.000124	.000065	.004	-.009	-.389
	62500444882.	15.850	6615.6	-.999812	-.000902	.00060		
	182.	.030	29.1	.000118	.000062	.004	-.009	-.390
	62500444568.	15.865	6592.2	-.999765	-.000996	.00055		
	167.	.028	26.6	.000109	.000057	.004	-.010	-.389
	62500444760.	15.879	6581.5	-.999687	-.001116	.00052		
	158.	.026	25.1	.000103	.000053	.004	-.009	-.388
	62500445107.	15.882	6561.8	-.999638	-.001238	.00058		
	176.	.029	27.8	.000114	.000059	.003	-.009	-.386
	62500444311.	15.904	6556.6	-.999574	-.001311	.00061		
	186.	.031	29.5	.000120	.000063	.004	-.010	-.387
	62500444355.	15.882	6591.7	-.999710	-.001578	.00055		
	168.	.028	26.7	.000109	.000057	.004	-.010	-.389
	62500444578.	15.865	6568.4	-.999670	-.001763	.00053		
	160.	.026	25.3	.000104	.000054	.004	-.009	-.386
Mean:	62500444554.	15.876	6581.5	-.999706	-.001059			
	316.	.014	16.2	.000064	.000408			
						ρ_1	ρ_2	ρ_3

Table 7

Example of an Output Protocol at 55.7 GHz (51pts/128avg):

- F3-fit Parameters (a′,a″; and S_R, f_x, g_x)
- Results for α_x (20) and N_x (21)
- Standard Deviation of the Residuals for Five- and Two-Parameter Fits, σ_s^a and σ_s^b

DRY AIR P = 0 to 760 to 0 torr 55.7 GHz, 29.4 C

S, Hz	a′	a″
1266.7	-.999517	.000165
5.2	.000050	.000111

P	f_x	g_x	α_x	N_x	σ_s^a	σ_s^b
torr	Hz		dB/km	ppm		
.0	55672046179.	83.911	.00	.000	.00028	.00075
	491.	.063	.00	.000		
9.1	55671880862.	83.502	.00	2.969	.00030	.00036
	222.	.107	.03	.010		
14.2	55671798401.	82.873	.00	4.451	.00027	.00085
	395.	.082	.02	.011		
22.4	55671637695.	83.217	.00	7.337	.00031	.00040
	50.	.088	.02	.009		
35.6	55671379879.	84.415	.12	11.968	.00029	.00052
	493.	.083	.02	.012		
57.0	55670968313.	84.547	.15	19.361	.00031	.00039
	245.	.087	.02	.010		
90.8	55670322132.	86.191	.53	30.968	.00029	.00061
	186.	.156	.04	.009		
145.9	55669267863.	86.086	.50	49.905	.00032	.00053
	235.	.151	.04	.010		
231.0	55667638428.	89.597	1.31	79.173	.00030	.00040
	344.	.109	.03	.011		
353.9	55665293637.	92.916	2.08	121.291	.00029	.00039
	293.	.174	.04	.010		
525.6	55662010579.	99.172	3.52	180.263	.00029	.00035
	385.	.132	.04	.011		
759.7	55657524400.	106.754	5.27	260.845	.00030	.00058
	433.	.167	.05	.012		
.0	55672043427.	84.068	.04	.149 = N_c	.00000	.00037
	165.	.134	.03	.009		

6. ATTENUATION RESULTS AND ERROR DISCUSSION

6.1 Data Format

Over 4,300 attenuation values $\alpha_x(f,P,T)$ have been measured. This large data base is presented in the Appendix, where it is organized in 12 sections (**A**. to **L**., RE) each for a fixed pressure value. Three temperature groups (7°, 30°, 52°C) exist, arranged from 53.9 to 66.3 GHz in 100 MHz increments (132f x 11P x 3T = 4,356). The condensed presentation reduces the two examples detailed in Sect. 5.4 to the following format:

SECTION **L**.	Summary	Individual Record	
	29.7(4)	55.65752	5.25(.05)
	759.8(2)	759.7	5.36[0.11]
	0.31	p. A-107	
	6.7(2)	60.66801	16.31(.03)
	759.9(2)	760.2	16.63[0.32]
	0.38	p. A-110	

Summary information for each group (n ≈ 130 frequencies) includes mean and standard deviation of all measured temperatures T_x [29.7(4)°C] and pressures P_x [759.8(2) torr]. Also given is the standard deviation σ_s (0.31 dB/km) of the mean of all (n) differences $\Delta\alpha$ (26) within a P,T-group. An individual record lists six values:

1) Measured frequency, f_x = 55.65752 GHz
2) Mean of the attenuation rate, α_x = 5.25 dB/km
3) Standard deviation, $\delta\alpha_x$ = .05 dB/km (F3 method)
4) Measured pressure, P_x = 759.7 torr
5) MPM89 prediction, α_M = 5.36 dB/km based on f_x, P_x, T_x
6) The difference (+0.11 dB/km) between predicted and measured values,

$$\pm \Delta\alpha = \alpha_M - \alpha_x \, . \tag{26}$$

6.2 Measurement Errors

Experimental errors are usually separated into random and systematic components. Random errors result from the residual noise inherent to the measurement process, which distributes successive data in a normal (Gaussian) sense about some mean. In the absence of systematic errors, this mean approaches the true value as the number of independent measurements increases. Electronic noise of the ANA causes signal fluctuations with elapsed time (see Fig. 7) which can be reduced by averaging the results of repeat measurements. The available capacity for data storage and the related increase in time duration for a full measurement sequence both set a practical limit on the number of repeat runs to ten.

Systematic errors in a measurement, such as mechanical changes in the resonator structure, cannot be described by statistical means. They produce a bias in the result, which (a) may be correctable, (b) remain uncorrected but can be included in the uncertainty statement, or in the worst case (c) go undetected and unknowingly affect the measurement. The error budget needs to be quantified to the level of the detection sensitivity, $d\alpha \approx \pm 0.02$ dB/km, which means signal changes of 2×10^{-3} ($0.02\cdot L_E$, = 0.0048 dB) and phase changes of 40 millidegrees have to be specified. By design, a laboratory experiment under well controlled conditions minimizes random and averts systematic errors. Measurement uncertainties of the experimental variables f, P, T, for example, contributed only negligible errors to the measured attenuation rate. The relationship (20) between recorded s_{11}-data and computed α_x-result is based on knowing the parameters S_R, g_0, and g_x. The three parameters were extracted by the method of least squares, which also provided their standard fitting errors (see Tables 6 and 7). Mean α_x and standard deviation $\delta\alpha_x$ were computed from the statistics of ten runs. Throughout the twelve data groups, the individual uncertainties $\delta\alpha_x$ exhibit, on the average, two distinct trends that reflect different measurement conditions:

First period,	f = 60 to 64 GHz,	$\delta\alpha_x \leq \pm 0.05$ dB/km
Second period,	f = 54 to 60 GHz,	$\delta\alpha_x \leq \pm 0.15$ dB/km.

The deterioration in measurement precision for the second production sequence was caused by our attempt to complete the experiments within a given time frame. In the first period, only five successive resonances under optimized (tuned) coupling conditions (8 to 3 percent) were detected, and the completion of a measurement series took a little more than an hour. In the second period, thirteen successive resonances were used, which extended the duration of a measurement series to over four hours. Since for these multi-frequency measurements the coupling factors got as low as 0.5 percent, the signal-to-noise ratio for s_{11} was not optimized.

On the other hand, the refractivity results of the first period proved unreliable. The mechanical coupler to the tuning micrometer transmitted stress motion into the resonator structure. The problem was corrected for the second period by disengaging the coupler. Reliable refractivity results ($\delta N_x \leq 0.02$ ppm) are available for future analysis on a similar scope that is demonstrated in the Appendix for attenuation rates.

After completing the scheduled experiments, a raw data base was available for analysis that consisted of $139(f_x) \times 12(P) \times 3(T) \approx 5{,}000$ attenuation values for dry air. A few measurement sequences were found to be corrupted by various experimental problems, leaving about 4,400 $\alpha_x(f_x,P,T)$-values of useful data, which are tabulated in the Appendix and for a large portion plotted in Figure 9 to give an overview. Although the logα-scale (Fig. 9) is deceiving, we notice generally good agreement with MPM predictions -- discrepancies exhibit roughly a ± 10 percent spread. We believe the new experimental data base has the potential to support adjustments to spectroscopic parameters of MPM89 to raise the consensus to a better than ±2 percent level. The rationale behind minor revisions of absorption data α_x due to small (± 0.25 dB/km) baseline corrections and their collective evaluation with respect to agreement with predictions close this report.

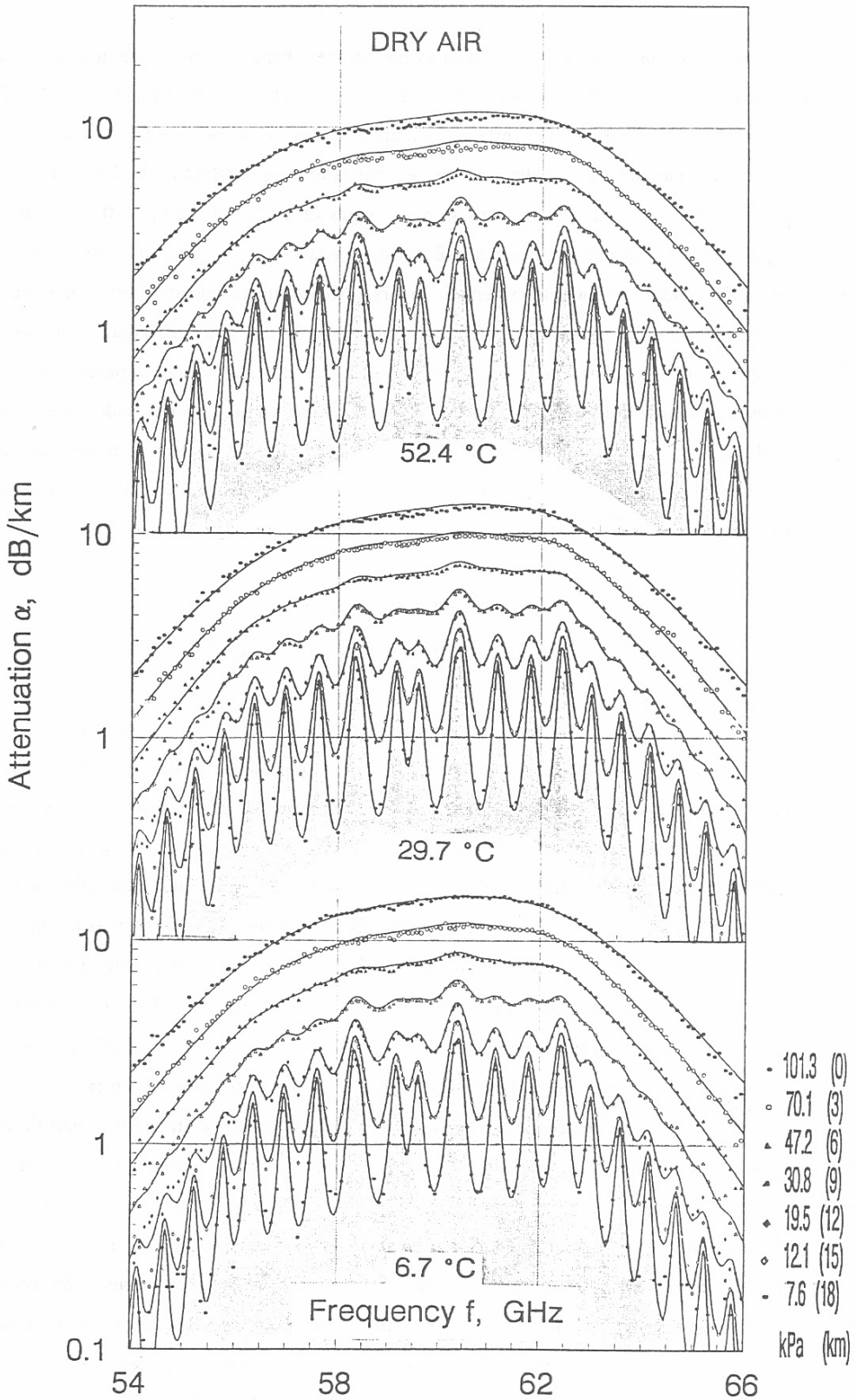

Figure 9. Overview of measured attenuation rates (symbols) and MPM89 predictions (solid lines) for dry air (f = 54-66 GHz, P = 7.6-101 kPa, T = 7,30,52°C; see Appendix **E.** - **L.**).

6.3 Baseline Behavior ($\alpha = 0$ at $P = 0$)

The evacuated ($P = 0$) spectrometer records $\alpha_x = 0.00 \pm 0.025$ dB/km over a 24-hr period if left unperturbed (see Fig. 7). However, each measurement series steps through a pressure sequence that begins with $P_i = 0$ and ends with $P_f = 0$. The baseline behavior $\alpha_x(P_f = 0)$ unmasks systematic errors that had occurred during the course of an experimental sequence (see RE - Appendix). The frequency distribution of the individual standard deviations $\delta\alpha_x$ for 139 α_x-values within a temperature group seemed nearly random with a zero mean. The standard deviation of that mean, σ_{Exp}, is listed in Table 8. Any pseudo-negative attenuation values were set equal to zero and the negative part added to the standard deviation, $\delta\alpha_x$. For example, $\alpha_x = -0.05(.04)$ was set to $\alpha = 0.00(.09)$ and $\alpha_M = 0.00[+0.05]$. About 95 percent of the individual values deviated from zero by no more than $\pm$ 0.25 dB/km; the remaining values were rejected as outliers.

Collective statistics of the data groups $\alpha_x(f_x, P)_T$ in the Appendix disclose certain sensitivities to various corrective measures. The first adjustment applied the inverse of one-half of the baseline signal to the original data, since at some point in the measurement sequence it actually had taken place. The standard deviation σ_{Exp} of the mean of $\Delta\alpha$ was reduced considerably to values σ_x; i.e., from about 0.1 to 0.05 dB/km (see Table 8). We report this "corrected" data set in the Appendix as final result of the experimental effort.

6.4 Data Manipulations

To investigate the systematic effects further, the hypothetical "true" attenuation $\alpha(f,P,T)$ was replaced by the predicted value $\alpha_M(f_x,P_x,T_x)$. Then various standard deviations σ of the mean of the collective data behavior, $\Sigma_n(\Delta\alpha)_n$, were computed to evaluate the effectiveness of data manipulations performed on the n groups of the data base. Correlated behavior of the difference $\Delta\alpha$ (26) between predicted and measured data, was used to selectively filter out random uncertainties of α_x and to extract information on systematic effects. Results of two different adjustments are listed in Table 9.

With the assistance of MPM89 one can identify systematic components in the collective experimental error (mean of $\delta\alpha_x$ related to incorrect model predictions (see Figs. A-1b to 11b). By making simple, though effective adjustments, it was possible to further reduce σ_x. The line positions (ν_k) of MPM89 were assumed to be correct; uncertainties are expected for strength, width, and overlap (S_k, γ_k, and I_k) parameters. When the strengths S_k and widths γ_k are correct, then one expects at low pressures ($P \leq 10$ kPa) over the limited frequency range of the isolated line shape ($\approx \nu_o \pm 10\gamma$) that the sum of the differences, $D = \Sigma n(\pm\Delta\alpha)_n \approx 0$. When the overlap coefficients I_k are correct, then one expects $D \approx 0$ at high pressures ($P \geq 50$ kPa) over the full band response ($\approx 60 \pm 30$ GHz). Since the results only cover 60 ± 8 GHz, one notices in the mean (Table 8) a bias increasing with pressure.

Linewidth Dependence: The standard deviation σ_n of $\Sigma_n(\Delta\alpha)_n$ for each of the three temperature sets is roughly a constant for P = 1 to 20 kPa that reduces (typically to $\sigma_c \approx 0.07$ dB/km), when (7) is modified to

$$(\gamma_{mod} = 1.05 \cdot \gamma_k \; . \qquad (27)$$

Table 8

Standard Deviations σ (dB/km) of the Mean of All Differences $\Delta\alpha$ (Prediction - Experiment) Within a Group of Attenuation Results $\alpha(f_x)_{P,T}$:

- Original Data and Baseline Adjustment -

H =	30	24	21	18	15	12	9	6	3	0	km	
P = 0	1	3	5	8	12	20	31	47	70	101	kPa	
σ_{Exp} for results $\alpha_{Exp}(f_x)_{P,T}$ [1]												Temp
.08	.08	.08	.08	.09	.09	.11	.11	.16	.23	.29		7°C
.11	.10	.11	.11	.11	.11	.13	.15	.19	.28	.42		30°C
.11	.10	.09	.09	.09	.11	.13	.18	.20	.33	.46		52°C
σ_x for baseline-corrected results $\alpha_x(f_x)_{P,T}$ [2]												
.04	.06	.06	.06	.08	.08	.08	.10	.15	.23	.31		7°C
mean .00	.00	.00	.00	.01	.02	.03	.06	.07	.08	.08		
.06	.07	.07	.07	.07	.08	.09	.09	.14	.19	.38		30°C
.00	.00	.00	.00	.01	.02	.03	.06	.09	.13	.19		
.05	.07	.06	.06	.07	.08	.08	.11	.15	.29	.43		52°C
.00	.00	.00	.00	.01	.02	.03	.07	.10	.18	.27		

[1] Each group is made up by original results, $\alpha_{Exp}(139\times f_x)_{P,T}$

[2] Each group is made up by edited results, $\alpha_x(132\times f_x)_{P,T}$ (outliers eliminated and baseline correction applied).

Table 9

Standard Deviations σ (dB/km) of the Mean of All Differences $\Delta\alpha$ (Prediction - Experiment) Within a Group of Attenuation Results $\alpha(f_x)_{P,T}$

- Adjustments to the Prediction Model -

H =	30	24	21	18	15	12	9	6	3	0	km	
P = 0	1	3	5	8	12	20	31	47	70	101	kPa	
σ_a (linewidth adjustment)[a] σ_x (see Table 8)												Temp
.04	.06	.06	.06	.07	.07	.07	.09	-	-	-		7°C
.04	.06	.06	.06	.08	.08	.08	.10					
.06	.07	.06	.06	.06	.07	.08	.08	-	-	-		30°C
.06	.07	.07	.07	.07	.08	.09	.09					
.05	.07	.06	.06	.06	.07	.08	.10	-	-	-		52°C
.05	.07	.06	.06	.07	.08	.08	.11					
σ_b (overlap adjustment)[b] σ_x (see Table 8)												
.04	-	-	-	-	-	.07	.08	.14	**.26**	**.51**		7°C
.04						.08	.10	.15	.23	.31		
.06	-	-	-	-	-	.08	.08	.10	.17	.37[c]		30°C
.06						.09	.09	.14	.19	.38[c]		
.05	-	-	-	-	-	.07	.09	.11	.20	.30		52°C
.05						.08	.11	.15	.29	.43		

[a] see Eqn (27)

[b] see Eqn (28)

[c] see Fig. 10 for - $\Delta\alpha$ data between 58 and 66 GHz

Overlap Dependence: Overlap effects become important as pressure P approaches one atmosphere. At P = 101 kPa = 1 atm, the standard deviation σ_x has increased to 0.31, 0.38, 0.43 dB/km at T_x = 7°, 30°, 52°C, respectively. These values change to 0.51 (worse), 0.37 (same), 0.30 (better), when (8) is modified to

$$I_{mod} = 0.80 \cdot I_k \ . \tag{28}$$

At 52°C, there is improvement, but not for the 7°C data. The temperature dependence of I_k needs to be reevaluated. Figure 10 shows an example (101 kPa, 30°C) of the individual differences $\Delta\alpha(f)$, plotted over a frequency range from 58 to 66 GHz for two sets of interference coefficients, $0.8 \cdot I_k$ and I_k. The distinction between random and systematic components is clearer and it remains a challenge to determine a better "I_k Set" that randomizes the difference distribution, $\Delta\alpha(f)$. Special fitting techniques need to be applied to infer revised spectrocopic parameter sets (2 × 38, Table 1) and associated temperature dependences for γ_k (7) and I_k (8) from the data base given in the Appendix.

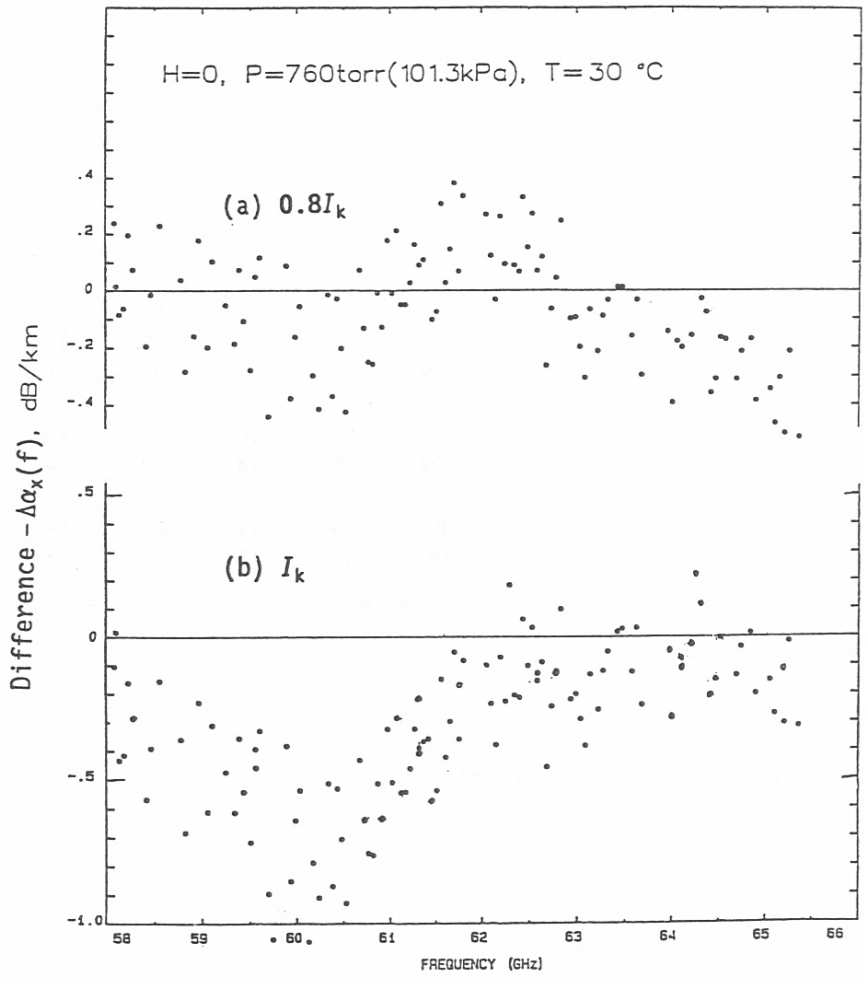

Figure 10. Differences between measured and predicted attenuation rates (α_x-α_M) from f = 58 to 66 GHz (101 kPa, 30°C) for two different model (MPM89) assumptions: (a) $0.8 \cdot I_k$ and (b) I_k (8).

7. CONCLUSIONS AND RECOMMENDATIONS

The 60-GHz oxygen spectrum dominates atmospheric radiative transfer roughly from 50 to 70 GHz. At altitudes below 30 km, an absorption band is formed by the overlap of more than thirty pressure-broadened lines. The spectral band shape is described by Equation (6). Interference (line coupling) effects take place when more than one spectral line contributes to an absorption value. In Rosenkranz's theory (1988), pressure-proportional interference parameters I_k alter the band shape in such a way that absorption is raised in the middle and lowered in the wings (see Fig. 3). Given pressure and temperature, absolute absorption by the $\mathbf{O}_2$ spectrum of dry air can be computed in terms of attenuation rates α (dB/km) by means of the MPM89 model that was detailed in Section 2. To check the model predictions, controlled laboratory experiments were prepared which simulate atmospheric pressure conditions below 30 km altitude in 3-km increments.

Two key components of the spectrometer setup were a Fabry-Perot resonator cell and an automatic network analyzer. Experimental principles, instrumental performance, examples of spectroscopic results, and the measurement uncertainties were discussed. The instrumental performance (sensitivity, stability, etc.) was much improved over past efforts (Newell and Baird, 1965; Poon, 1977; Liebe and Layton, 1987; Read et al., 1988) by taking advantage of recent advances in millimeter-wave instrumentation. A microcomputer was used to handle multiple tasks including spectrometer control, individual data acquisition totaling a number exceeding 10^9, and data reduction.

Measurements were performed at frequencies between 53.9 and 66.3 GHz in 100 MHz steps at three temperatures (7,30,52°C) for eleven selected pressures values (1.2-101 kPa). More than 4,000 attenuation rates α were deduced from the measurement series. Fluctuations of the detection level ($\leq \pm$ 0.05 dB/km) were a main cause for experimental uncertainty. The total relative errors were estimated to be typically smaller than ± 2 percent for attenuation rates between 2 and 20 dB/km. Selected results of α(f,P,T) were displayed in Figure 9, and the more complete set is presented numerically and graphically in the Appendix.

A first comparison of the detailed attenuation results with predictions revealed discrepancies which correlate with width and overlap parameters. Also, systematic over-predictions in the middle of the band seem to depend on temperature (e.g., at 60 GHz, 30-101 kPa, the relative error increases from about 2 % at 7°C to 8 % at 52°C). The extensive data set is suitable to support efforts aimed at improving the molecular data base for the atmospheric 60-GHz oxygen spectrum. The MPM89 model can serve as a selective filter to separate random measurement errors from incorrect model predictions. A reliable model is particularly valuable to atmospheric radiative transfer problems (Rosenkranz, 1991).

Additional, related work on the atmospheric 60-GHz $\mathbf{O}_2$ spectrum is recommended in three areas: (a) analyze the refractivity data which supplement many attenuation results and use the complete complex evidence to improve on the width and interference parameter sets; (b) continue measurement series at subfreezing temperatures (5 to -50°C) to simulate real atmospheric conditions; and (c) study the Zeeman effect of isolated $\mathbf{O}_2$ lines at low pressures ($\leq$ 5 kPa) with high frequency resolution (0.01 to 10 MHz) under controlled simulations of the geomagnetic field.

8. REFERENCES

Danese, L., Partridge, R. B. (1989), Atmospheric emission models: confrontation between observational data and predictions in the 2.5 - 300 GHz frequency range, *Astrophys. J.,* 342, pp. 604-615.

Hill, R. J. (1987), Absorption by the tails of the oxygen microwave resonances at atmospheric pressures, *IEEE Trans. Ant. Propag.,* AP-35, no. 2, pp. 198-204.

Hufford, G. H., Liebe, H. J. (1989), Millimeter-wave propagation in the mesosphere, *NTIA-Report 89-249*, September, 62 pp. (NTIS Order No. PB 90-119868/AS).

Liebe, H. J., G. G. Gimmestad, and J. D. Hopponen (1977), Atmospheric oxygen microwave spectrum - experiment versus theory, *IEEE Trans. Ant. Propag.,* AP-25, no.3, pp. 327-355; and *Proc. Int. Symp. URSI-F,* May, LaBaule, France, pp. 619-624.

Liebe, H. J., V. L. Wolfe, and D. A. Howe (1984), Test of wall coatings for controlled moist air experiments, *Rev. Sci. Instr.,* 55, no. 10, pp. 1702-1705.

Liebe, H. J. and D. Layton (1987), Millimeter-wave properties of the atmosphere: Laboratory studies and propagation modeling, *NTIA-Report* 87-224, September, 80 pp. (NTIS Order No. PB 88-164215/AF).

Liebe, H. J. (1985), An updated model for millimeter-wave propagation in moist air, *Radio Science,* 20, no. 5, pp. 1069-1089.

Liebe, H. J. (1989), MPM - an atmospheric millimeter-wave propagation model, *Int. J. IR & MM Waves,* 10, no. 6, pp. 631-650.

Marquardt, D. W. (1963), An algorithm for least-squares estimation of nonlinear parameters, *J. Soc. Indust. Appl. Math.,* 11, no. 2, pp. 431-441.

Newell, A. C. and R. C. Baird (1965), Absolute determination of refractive indices of gases at 47.7 GHz, *J. Appl. Phys.,* 36, no. 12, pp. 3751-3759.

Poon, R. K. (1977), Microwave absorption of oxygen measured with a Fabry-Perot spectrometer, *J. Quant. Spectr. Radiat. Transf,* 17, pp. 561-569.

Read, W. G., K. W. Hillig II, E. A. Cohen, and H. M. Pickett (1988), The measurement of absolute absorption of millimeter radiation in gases: The absorption of CO and O_2, *IEEE Trans. Ant. Propag.,* AP-36, no. 8, pp. 1136-1143.

Rosenkranz, P. W. (1988), Interference coefficients for overlapping oxygen lines in air, *J. Quant. Spectr. Rad. Tranf,* 39, no. 4, pp. 287-297.

Rosenkranz, P. W. (1991), Absorption of microwaves by atmospheric gases: chapter 2 in *Atmospheric Remote Sensing By Microwave Radiometry,* M. A. Janssen (ed.), (Wiley-Interscience, NY).

Schulten, G. (1966), Resonatoren für Millimeterwellen und ihre Anwendung zur Beobachtung von Gasresonanzen, *FREQUENZ,* 20, no. 1, pp. 10-22.

Zink, L. R., Mizushima, M. (1987), Pure rotational far-infrared transitions of $^{16}O_2$ in its electronic and vibrational ground state, *J. Molec. Spectr.,* 125, pp. 154-158.